Nonadiabatic Kohn Anomaly in Heavily Boron-Doped Diamond

Fabio Caruso,[1,6] Moritz Hoesch,[2] Philipp Achatz,[3] Jorge Serrano,[4] Michael Krisch,[5] Etienne Bustarret,[3] and Feliciano Giustino[1,*]

[1]*Department of Materials, University of Oxford, Parks Road, Oxford, OX1 3PH, United Kingdom*
[2]*Diamond Light Source, Harwell Campus, Didcot OX11 0DE, United Kingdom*
[3]*Université Grenoble Alpes, CNRS, Institut NEEL, F-38000 Grenoble, France*
[4]*Yachay Tech University, School of Physical Sciences and Nanotechnology, 100119-Urcuquí, Ecuador*
[5]*European Synchrotron Radiation Facility, 6 rue Jules Horowitz, 38043 Grenoble Cedex, France*
[6]*Institut für Physik and IRIS Adlershof, Humboldt-Universität zu Berlin, Berlin, Germany*

(Received 14 November 2016; published 6 July 2017)

We report evidence of a nonadiabatic Kohn anomaly in boron-doped diamond, using a joint theoretical and experimental analysis of the phonon dispersion relations. We demonstrate that standard calculations of phonons using density-functional perturbation theory are unable to reproduce the dispersion relations of the high-energy phonons measured by high-resolution inelastic x-ray scattering. On the contrary, by taking into account nonadiabatic effects within a many-body field-theoretic framework, we obtain excellent agreement with our experimental data. This result indicates a breakdown of the Born-Oppenheimer approximation in the phonon dispersion relations of boron-doped diamond.

DOI: 10.1103/PhysRevLett.119.017001

The Kohn anomaly (KA) is one of the most striking manifestations of the influence of electron-phonon coupling on the lattice dynamics of metals [1]. KAs result from the screening of lattice vibrations by virtual electronic excitations across the Fermi surface [2] and manifest themselves through distinctive dips in the phonon dispersion relations. The existence of KAs was confirmed by inelastic neutron scattering experiments [3] shortly after Kohn's theoretical prediction [1]. Since then, KAs have been observed in a number of metals [4–6] and conventional superconductors [7,8], as well as superconducting semiconductors [9].

Interest in KAs was recently reignited by the discovery of *nonadiabatic* KAs in carbon materials, such as graphene [10,11], carbon nanotubes [12,13], and graphite intercalation compounds [14–16]. At variance with adiabatic KAs, which are well described in the adiabatic Born-Oppenheimer approximation [1], nonadiabatic KAs arise when the electronic screening takes place on time scales which are comparable to the period of lattice vibrations, and signal the breakdown of the Born-Oppenheimer approximation. In the majority of current first-principles calculations, these nonadiabatic effects are ignored on the grounds that they should be of the order of m/M, with m the electron mass and M the characteristic nuclear mass. While the calculations of nonadiabatic phonon linewidths may be performed using standard implementations [17], first-principles studies of renormalization effects on the phonon dispersions due to nonadiabaticity are extremely challenging and have thus far been confined to low-dimensional compounds. In particular, for metallic compounds characterized by a two-dimensional, quasi-two-dimensional, or one-dimensional structure, it has been shown that nonadiabatic effects can alter significantly the phonon dispersion relations [10–16,18]. Instead, for three-dimensional bulk metals, it has been suggested that nonadiabatic effects might be too small to be observable in an experiment [15].

The strong coupling between electrons and longitudinal optical (LO) phonons in diamond, manifested, for instance, by a 0.6 eV zero-point motion band-gap renormalization [19–21] and the emergence of type-II superconductivity for sufficiently high B doping [22], make it a good candidate for the observation of nonadiabatic effects in the phonon dispersions. Pristine diamond has previously attracted considerable interest due to the anomalous overbending of the optical phonon branch [23]. In the presence of B dopants, the electron-phonon interaction induces a softening of the LO phonons at long wavelengths and a concomitant broadening of the spectral lines [9,24]. These effects are taken to be the signatures of a doping-induced KA. The measured softening is found to be between 4 and 7 meV for B-doping concentrations of 10^{20}–10^{21} cm^{-3} [9,24]. Intriguingly, first-principles calculations [25–29] gave a considerably more pronounced phonon softening, in the range of 20–30 meV. This unusually large discrepancy between the experiment and theory remains an outstanding question in the physics of superconducting diamond [30]. This led us to formulate the hypothesis that in order to explain the measured KA in diamond it might be necessary to invoke nonadiabatic effects.

In this work, we analyze the dispersion relations of the LO phonons of B-doped diamond using state-of-the-art first-principles calculations and inelastic x-ray scattering (IXS) measurements. By comparing the theory and experiment, we demonstrate that the nonadiabatic correction to the LO phonon energy is indeed very large, up to 10 meV. After including nonadiabatic effects within a field-theoretic framework, we

obtain an unprecedented agreement between the theory and experiment, and we resolve the discrepancy between earlier theoretical works and measured phonon dispersions. Our results demonstrate a breakdown of the adiabatic Born-Oppenheimer approximation in the phonon dispersion relations of boron-doped diamond, revealing that these effects may be sizable also in three-dimensional bulk compounds.

The B-doped diamond samples were prepared by microwave plasma-enhanced chemical vapor deposition from a hydrogen-rich gas phase with added diborane (B_2H_6). The samples were grown homoepitaxially on type Ib synthetic crystals with (001)-oriented surfaces at thicknesses of 25 ± 5 μm [31]. The boron concentration was determined from secondary ion mass spectroscopy (SIMS) of $^{11}B^-$, $^{12}C^-$, and $^{11}B^{12}C^-$ ions. For a B-doping concentration of 1.4×10^{21} cm^{-3}, the samples exhibit superconducting behavior with critical temperature $T_c = 2.8$ K. IXS spectra were measured at beam line ID28 at the European Synchrotron Radiation Facility (ESRF) with an energy resolution of 3.2 meV. The samples were aligned with the beam directed parallel to the surface and passing through the substrate or the B-doped diamond film, for measurements of pristine diamond and B-doped diamond, respectively. The scattering vector $\mathbf{Q}$ was varied from $(2.06, 0, 0)2\pi/a$ (close to Γ) to $(3, -0.12, 0)2\pi/a$ (close to X), with $a = 3.67$ Å. The small deviations in the $(0, k, 0)$ direction are given in Supplemental Table I [32]. The measured IXS spectra are shown in Figs. 1(c)–1(e) as heat maps and in Supplemental Fig. 1 as individual scans [32]. For the undoped case, our measurements are in excellent agreement with previous experimental data [33].

Nonadiabatic phonon dispersions were computed from first principles within the many-body theory of electron-phonon coupling. Nonadiabatic effects were accounted for via the phonon self-energy $\Pi^{\mathrm{NA}}_{\mathbf{q}\nu}$ [17]:

$$\hbar\Pi^{\mathrm{NA}}_{\mathbf{q}\nu}(\omega) = 2\sum_{mn}\int \frac{d\mathbf{k}}{\Omega_{\mathrm{BZ}}} g^{b}_{mn,\nu}(\mathbf{k},\mathbf{q}) g^{*}_{mn,\nu}(\mathbf{k},\mathbf{q}) \times \left(\frac{f_{n\mathbf{k}} - f_{m\mathbf{k}+\mathbf{q}}}{\epsilon_{m\mathbf{k}+\mathbf{q}} - \epsilon_{n\mathbf{k}} - \hbar(\omega + i\eta)} - \frac{f_{n\mathbf{k}} - f_{m\mathbf{k}+\mathbf{q}}}{\epsilon_{m\mathbf{k}+\mathbf{q}} - \epsilon_{n\mathbf{k}}}\right), \quad (1)$$

where $\epsilon_{n\mathbf{k}}$ and $f_{n\mathbf{k}}$ denote single-particle energies and Fermi-Dirac occupation factors, respectively, η is a positive infinitesimal, and Ω_{BZ} is the Brillouin zone volume. The *screened* electron-phonon matrix elements $g_{mn,\nu}(\mathbf{k},\mathbf{q})$ were obtained as $g_{mn,\nu}(\mathbf{k},\mathbf{q}) = (\hbar/2M\omega_{\mathbf{q}\nu})^{1/2}\langle\psi_{m\mathbf{k}+\mathbf{q}}|\partial_{\mathbf{q}\nu}V|\psi_{n\mathbf{k}}\rangle$, where $\psi_{n\mathbf{k}}$ denote Kohn-Sham single-particle eigenstates, M the C mass,

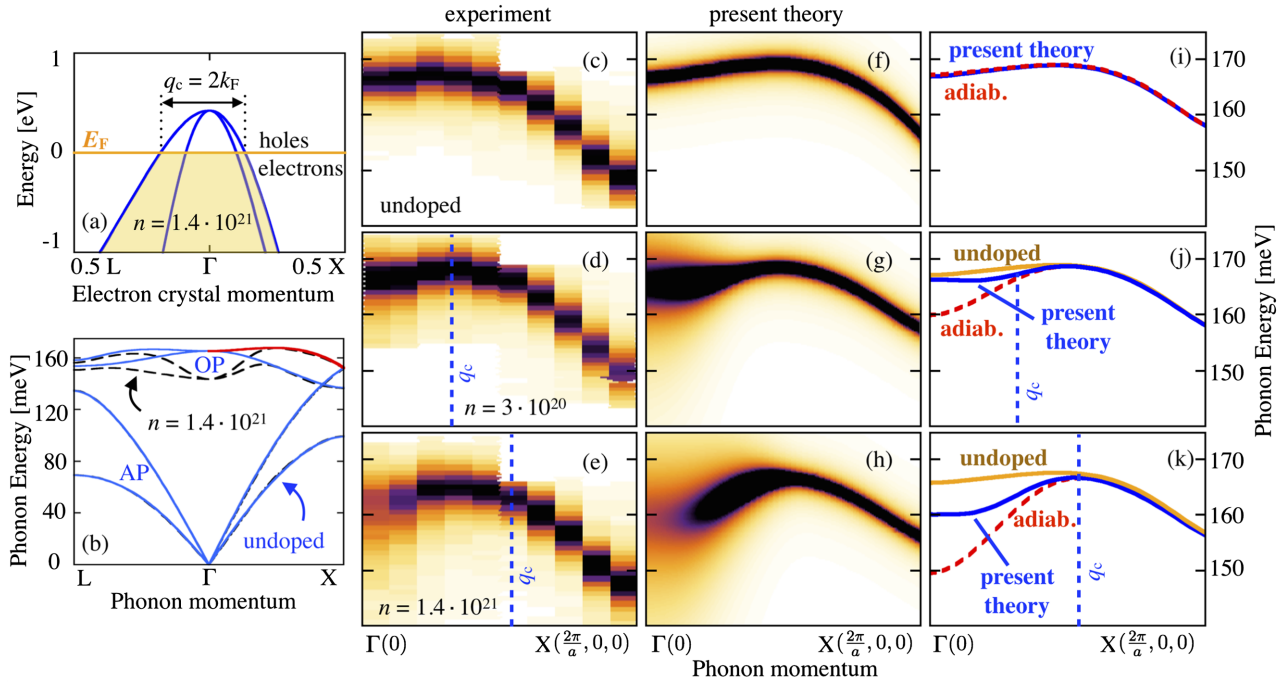

FIG. 1. (a) Density-functional theory band structure of diamond for a B concentration of 1.4×10^{21} cm^{-3}. (b) Adiabatic phonon dispersions of pristine (blue lines) and B-doped diamond (dashed black lines) for momenta along L-Γ-X, as obtained from density-functional perturbation theory. (c)–(e) Measured IXS spectra of pristine and B-doped diamond. The critical momentum for the onset of the KA, $q_c = 2k_F$, is indicated by vertical dashed lines; see also (a). (f)–(h) Nonadiabatic spectral function, obtained from Eqs. (1) and (2), for the LO phonon of (c) pristine and (d),(e) B-doped diamond along Γ-X. The phonon branch considered here is marked by the red line in panel (b). (i)–(k) Phonon energies obtained from Eq. (3) in the adiabatic approximation ($\Pi^{\mathrm{NA}}_{\mathbf{q}\nu} = 0$) and from the fully nonadiabatic theory (present theory). Nonadiabatic phonon dispersions of undoped diamond are reported for comparison. All doping concentrations are in units of cm^{-3}.

and $\partial_{\mathbf{q}\nu}V$ the derivative of the self-consistent potential associated with the νth phonon mode with wave vector $\mathbf{q}$ and energy $\hbar\omega_{\mathbf{q}\nu}$. $g_{mn,\nu}(\mathbf{k},\mathbf{q})$ is obtained from the *bare* matrix element $g^b_{mn,\nu}(\mathbf{k},\mathbf{q})$ by screening the variation of the ionic potential using the electronic dielectric function. Here we calculate $g^b_{mn,\nu}(\mathbf{k},\mathbf{q})$ by unscreening $g_{mn,\nu}(\mathbf{k},\mathbf{q})$ and neglect local-field effects for simplicity. Equation (1) accounts for both the screened and the bare electron-phonon vertices (g and g^b), and it thus avoids the approximation employed in previous first-principles calculations, whereby the matrix elements $g^b_{mn,\nu}(\mathbf{k},\mathbf{q})g^*_{mn,\nu}(\mathbf{k},\mathbf{q})$ were replaced by $|g_{mn,\nu}(\mathbf{k},\mathbf{q})|^2$ [17]. The nonadiabatic phonon dispersions, that is, the dispersions modified by the phonon self-energy of Eq. (1), were extracted directly from the phonon spectral function [34]:

$$A_{\mathbf{q}\nu}(\omega)=\pi^{-1}\mathrm{Im}\left[\frac{2\omega_{\mathbf{q}\nu}}{\omega^2-\omega^2_{\mathbf{q}\nu}-2\omega_{\mathbf{q}\nu}\Pi^{\mathrm{NA}}_{\mathbf{q}\nu}(\omega)}\right]. \quad (2)$$

Equation (2), which constitutes the phonon counterpart of the electronic spectral function [2], exhibits peaks at the nonadiabatic phonon frequencies $\Omega_{\mathbf{q}\nu}$ given by

$$\Omega^2_{\mathbf{q}\nu}\simeq\omega^2_{\mathbf{q}\nu}+2\omega_{\mathbf{q}\nu}\mathrm{Re}\Pi^{\mathrm{NA}}_{\mathbf{q}\nu}(\Omega_{\mathbf{q}\nu}), \quad (3)$$

with a full width at half maximum $\Gamma_{\mathbf{q}\nu}=2\hbar\mathrm{Im}\Pi^{\mathrm{NA}}_{\mathbf{q}\nu}(\Omega_{\mathbf{q}\nu})$. Nonadiabatic phonon spectral functions obtained from Eq. (2) are reported in Figs. 1(f)–1(h), whereas the phonon dispersions derived from Eq. (3) are shown in Figs. 1(i)–1(k).

An inspection of Eq. (1) reveals that nonadiabatic effects may become important whenever the transition energies between occupied and empty electronic states ($\epsilon_{m\mathbf{k}+\mathbf{q}}-\epsilon_{n\mathbf{k}}$) approach the characteristic phonon energy $\hbar\omega_{\mathbf{q}\nu}$. As in solids $\hbar\omega_{\mathbf{q}\nu}$ is typically $\lesssim$100 meV, this condition is satisfied only in metals, doped semiconductors, and narrow-gap semiconductors, wherein low-energy intraband transitions may be excited. Therefore, in these systems one may expect to observe (i) phonon damping effects, with a characteristic time scale set by the phonon lifetime $\tau_{\mathbf{q}\nu}=\hbar/\Gamma_{\mathbf{q}\nu}$, and (ii) a renormalization of the adiabatic phonon frequencies, arising from the finite value of $\mathrm{Re}\Pi^{\mathrm{NA}}_{\mathbf{q}\nu}(\Omega_{\mathbf{q}\nu})$ in Eq. (3). On the other hand, the standard Born-Oppenheimer approximation is recovered in the limit $\Pi^{\mathrm{NA}}_{\mathbf{q}\nu}=0$.

Calculations were performed using density-functional theory (ground state and band structures) and density-functional perturbation theory (phonon dispersion relations and electron-phonon matrix elements), using Quantum Espresso [38], EPW [44], and WANNIER90 [42]. The doping was modeled in the rigid-band approximation, and the spectral functions were computed at 300 K. Complete calculation details are given in Ref. [34]. The phonon dispersions of pristine diamond in the adiabatic approximation are presented in Fig. 1(b) for momenta along the L-Γ-X path. The acoustic and optical phonon branches, which correspond to the in- and out-of-phase oscillation of the diamond sublattices, are denoted as AP and OP, respectively, in Fig. 1(b). Pristine diamond is an insulator with a fundamental band gap $E_g=5.4$ eV [45,46], and the large optical phonon energy of $\hbar\omega_{\mathrm{ph}}=164$ meV reflects the stiffness of its covalent bonds. Since $E_g\gg\hbar\omega_{\mathrm{ph}}$, nonadiabatic effects are relatively unimportant, and the nonadiabatic corrections are smaller than 0.4 meV; see Fig. 1(i). The resulting phonon dispersions are in excellent agreement with our measured IXS spectrum in Fig. 1(c), in line with the notion that phonons in wide-band-gap insulators are well described in the adiabatic approximation.

To quantify the importance of nonadiabaticity for undoped semiconductors and insulators, we derive a simple estimate of the energy renormalization. In the limit of nondispersive electronic bands, one may replace $\epsilon_{m\mathbf{k}+\mathbf{q}}-\epsilon_{n\mathbf{k}}=E_g$ in Eq. (1). If we further assume an Einstein model for the optical phonons $\hbar\omega_{\mathbf{q}\nu}=\hbar\omega_E$ and we restrict ourselves to the limit $\hbar\omega_E\ll E_g$, the term in large parentheses in Eq. (1) reduces to $\hbar\omega_E/E_g^2$ to first order. An explicit approximation for Eq. (1) then is promptly obtained: $\hbar\Pi=2\epsilon_\infty g^2\hbar\omega_E/E_g^2$, with ϵ_∞ being the dielectric constant and g the average electron-phonon matrix element. For diamond, using $\epsilon_\infty=5.44$, $E_g=5.4$ eV, $\hbar\omega_E=0.16$ eV, and $g=0.1$ eV, we obtain $\hbar\Pi=0.5$ meV, which is consistent with the first-principles calculations shown in Fig. 1(i).

As compared to the undoped case, the IXS spectra of B-doped diamond in Figs. 1(d) and 1(e) exhibit a redshift of the LO phonon energy and an increase of the phonon linewidth close to Γ, which indicate the emergence of a doping-induced KA. To quantify the effect of doping on the phonon energy, we define the phonon-softening parameter $\Delta\Omega_{\mathbf{q}\nu}(n)=\Omega_{\mathbf{q}\nu}(0)-\Omega_{\mathbf{q}\nu}(n)$, where $\Omega_{\mathbf{q}\nu}(n)$ denotes the phonon frequency at a carrier density n. The softening and linewidth become more pronounced with the increase of doping concentration. The KA is observed only for wave vectors smaller than a critical cutoff value $q_c=2k_F$, with k_F being the Fermi momentum, which corresponds to the maximum momentum transfer for electron-phonon scattering on the Fermi surface; see Fig. 1(a) [1]. Using the Fermi momentum of the homogeneous electron gas model, $k_F=(3\pi^2n/N_m)^{1/3}$, where $N_m=3$ is the degeneracy of the valence-band top of diamond, we obtain $q_c=0.3$ and 0.5 Å^{-1} for doping levels of 3×10^{20} and 1.4×10^{21} cm^{-3}, respectively. These values are marked by vertical dashed lines in Figs. 1(d), 1(e), 1(j), and 1(k).

For momenta $q<q_c$, we find adiabatic phonon dispersions consistent with previous works [25,28,29]. As reported in Refs. [9,29], however, the adiabatic approximation leads to a systematic underestimation of the phonon energy as compared to the experiment, which becomes

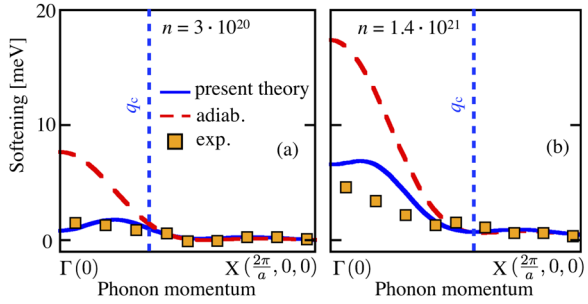

FIG. 2. Energy renormalization of the longitudinal optical phonons of diamond, for doping concentrations of (a) 1.4×10^{21} cm^{-3} and (b) 3×10^{20} cm^{-3}: experiment (squares) and adiabatic (dashed red line) and nonadiabatic theory (blue line).

more pronounced with the increase of doping concentration. Conversely, fully nonadiabatic calculations yield phonon energies in excellent agreement with IXS, as revealed by the comparison between Figs. 1(d) and 1(e) and Figs. 1(j) and 1(k). To quantify the importance of nonadiabatic effects, we compare in Fig. 2 the softening $\Delta\Omega_{\mathbf{q}\nu}$ and the line shapes for the LO phonon of B-doped diamond, as obtained from IXS, from the adiabatic approximation and from fully nonadiabatic calculations. Above the threshold $q > q_c$ for the onset of the KA, the theory and experiment yield a phonon softening smaller than 1 meV for all doping concentrations. For $q < q_c$, instead, the positive phonon softening reflects the redshift of the phonon frequency induced by electron-phonon interactions. Figures 2(a) and 2(b) reveal that the adiabatic approximation overestimates the experimental softening by as much as 300% close to Γ. At a doping concentration of 1.4×10^{21} cm^{-3}, for instance, the adiabatic LO phonon energy at Γ is softened by $\Delta\Omega_{\Gamma}^{\mathrm{adiab}} = 22$ meV, whereas from IXS we have $\Delta\Omega_{\Gamma}^{\mathrm{exp}} = 5.3$ meV. The nonadiabatic theory, on the other hand, yields a softening in excellent agreement with the experiment: For instance, we obtain $\Delta\Omega_{\Gamma}^{\mathrm{NA}} = 7$ meV for the same doping level. These results are further corroborated by considering an Einstein phonon model coupled to a homogeneous electron gas with parabolic dispersion $\epsilon_{\mathbf{k}} = \hbar^2 k^2 / 2m^*_{\mathrm{dos}}$, with $m^*_{\mathrm{dos}} = 1.18$ being the density-of-state effective mass of diamond. Within these approximations, Eq. (1) reduces to $\hbar\Pi = 2g^2\epsilon_\infty[\chi_0(\omega_E) - \chi_0(0)]$, with $\chi_0(\omega)$ being the long-wavelength limit ($\mathbf{q} \to 0$) of the Lindhard function [2]. For diamond, using $\hbar\omega_E = 0.16$ eV, $g = 0.1$ eV, $m^*_{\mathrm{dos}} = 1.18$, and $\epsilon_\infty = 5.44$, we obtain $\hbar\Pi \simeq 8$ meV for $n = 1.4 \times 10^{21}$ cm^{-3}, in agreement with our *ab initio* calculations.

These features are also nicely reproduced by the phonon dispersions reported in Figs. 1(g) and 1(h), confirming the nonadiabatic character of the KA. Owing to the undamped nature of phonons in the adiabatic approximation (here we ignore phonon-phonon interactions), the adiabatic spectral functions are characterized by infinitesimal linewidths. The nonadiabatic spectra, on the other hand, correctly reproduce (i) the increase of the spectral linewidth with doping concentration and (ii) the decrease of the linewidth with phonon momentum as shown in Figs. 1(c)–1(h) and in Fig. S3 [32]. The resulting spectral line shapes are in good qualitative agreement with IXS, suggesting that electron-phonon scattering constitutes the primary mechanism for LO phonon damping in superconducting diamond.

The pronounced nonadiabatic character of the lattice dynamics in doped diamond indicates a breakdown of the adiabatic Born-Oppenheimer approximation. This effect may be explained by considering the time scales involved: While LO phonons oscillate with a period $\tau_{\mathrm{ph}} = 25$ fs, the time scale of electronic screening τ_s is set by the plasma frequency ω_{pl} via $\tau_s = 2\pi/\omega_{\mathrm{pl}} = 2\pi(4\pi n/m^*\epsilon_\infty)^{-1/2}$, with m^* being the carrier effective mass. Using this expression, we find $\tau_s = 9$ and 4 fs for $n = 3 \times 10^{20}$ and 1.4×10^{21} cm^{-3}, respectively, which are compatible with the results of optical measurements [47,48]. As screening operates on time scales that approach the characteristic phonon period, the assumptions underlying the Born-Oppenheimer approximation are not valid, and we see the emergence of strong nonadiabatic coupling.

As a first step to explore the consequences of nonadiabaticity in B-doped diamond, we examine the superconducting critical temperature T_c using McMillan's formula [49,50]: $T_c = \langle\omega\rangle/1.2 \exp\{-1.04(1+\lambda)/[\lambda - \mu^*(1+0.62\lambda)]\}$, where λ is the electron-phonon coupling strength and $\langle\omega\rangle$ the logarithmic average of the phonon frequency. Following Refs. [50,51], the Coulomb pseudopotential μ^* is set to the standard value of 0.11. Noting that $\lambda \propto \omega_{\mathbf{q}\nu}^{-2}$ [17], a small change in the phonon frequency, as introduced by the adiabatic approximation, may induce a large modification of T_c. At a doping concentration of 1.4×10^{21} cm^{-3}, for instance, the adiabatic approximation underestimates the LO phonon frequency in diamond by ~10%. In turn, this results in an overestimation of λ by ~20%. This inaccuracy is amplified by the exponential dependence of T_c on λ, leading to an overestimation of the critical temperature by up to 50%. Nonadiabatic effects thus carry important implications for the theoretical prediction of T_c and should be considered in future studies.

In conclusion, by combining first-principles calculations of the electron-phonon interaction and high-resolution IXS experiments, we demonstrated the emergence of a nonadiabatic KA in superconducting diamond. Beside resolving a long-standing discrepancy between the theory and experiment, these findings reveal that a breakdown of the Born-Oppenheimer approximation may lead to sizable renormalization effects in the phonon dispersions of three-dimensional crystals. Our work calls for a systematic investigation of nonadiabatic effects and Kohn anomalies in the phonon dispersions of three-dimensional heavily doped semiconductors as well as superconducting oxides.

We thank L. Ortéga for help with the x-ray diffraction characterization of the samples and F. Jomard for calibration of the B concentration by SIMS and depth profiling a few micrometers. The research leading to these results has received funding from the Leverhulme Trust (Grant No. RL-2012-001), the European Union's Horizon 2020 research and innovation program under Grant Agreement No. 696656—GrapheneCore1, and the United Kingdom Engineering and Physical Sciences Research Council (Grant No. EP/J009857/1). Supercomputing time was provided by the University of Oxford Advanced Research Computing facility and the ARCHER United Kingdom National Supercomputing Service. We acknowledge the ESRF for granting use of beam line ID28, which contributed to the results presented here.

*feliciano.giustino@materials.ox.ac.uk

[1] W. Kohn, Phys. Rev. Lett. **2**, 393 (1959).
[2] G. Mahan, *Many-Particle Physics* (Springer, New York, 2000).
[3] B. N. Brockhouse, K. R. Rao, and A. D. B. Woods, Phys. Rev. Lett. **7**, 93 (1961).
[4] B. N. Brockhouse, T. Arase, G. Caglioti, K. R. Rao, and A. D. B. Woods, Phys. Rev. **128**, 1099 (1962).
[5] Y. Nakagawa and A. D. B. Woods, Phys. Rev. Lett. **11**, 271 (1963).
[6] S. H. Koenig, Phys. Rev. **135**, A1693 (1964).
[7] A. Q. R. Baron, H. Uchiyama, Y. Tanaka, S. Tsutsui, D. Ishikawa, S. Lee, R. Heid, K.-P. Bohnen, S. Tajima, and T. Ishikawa, Phys. Rev. Lett. **92**, 197004 (2004).
[8] P. Aynajian, T. Keller, L. Boeri, S. M. Shapiro, K. Habicht, and B. Keimer, Science **319**, 1509 (2008).
[9] M. Hoesch, T. Fukuda, J. Mizuki, T. Takenouchi, H. Kawarada, J. P. Sutter, S. Tsutsui, A. Q. R. Baron, M. Nagao, and Y. Takano, Phys. Rev. B **75**, 140508 (2007).
[10] M. Lazzeri and F. Mauri, Phys. Rev. Lett. **97**, 266407 (2006).
[11] S. Pisana, M. Lazzeri, C. Casiraghi, A. K. Novoselov, K. S. Geim, A. C. Ferrari, and F. Mauri, Nat. Mater. **6**, 198 (2007).
[12] N. Caudal, A. M. Saitta, M. Lazzeri, and F. Mauri, Phys. Rev. B **75**, 115423 (2007).
[13] S. Piscanec, M. Lazzeri, J. Robertson, A. C. Ferrari, and F. Mauri, Phys. Rev. B **75**, 035427 (2007).
[14] M. Calandra, M. Lazzeri, and F. Mauri, Physica (Amsterdam) **456C**, 38 (2007).
[15] A. M. Saitta, M. Lazzeri, M. Calandra, and F. Mauri, Phys. Rev. Lett. **100**, 226401 (2008).
[16] M. Calandra, G. Profeta, and F. Mauri, Phys. Rev. B **82**, 165111 (2010).
[17] F. Giustino, Rev. Mod. Phys. **89**, 015003 (2017).
[18] M. Leroux, I. Errea, M. Le Tacon, S.-M. Souliou, G. Garbarino, L. Cario, A. Bosak, F. Mauri, M. Calandra, and P. Rodière, Phys. Rev. B **92**, 140303 (2015).
[19] F. Giustino, S. G. Louie, and M. L. Cohen, Phys. Rev. Lett. **105**, 265501 (2010).
[20] E. Cannuccia and A. Marini, Phys. Rev. Lett. **107**, 255501 (2011).
[21] G. Antonius, S. Poncé, P. Boulanger, M. Côté, and X. Gonze, Phys. Rev. Lett. **112**, 215501 (2014).
[22] E. A. Ekimov, V. A. Sidorov, E. D. Bauer, N. N. Mel'nik, N. J. Curro, J. D. Thompson, and S. M. Stishov, Nature (London) **428**, 542 (2004).
[23] M. Schwoerer-Böhning, A. T. Macrander, and D. A. Arms, Phys. Rev. Lett. **80**, 5572 (1998).
[24] E. Bustarret, Physica (Amsterdam) **514C**, 36 (2015).
[25] L. Boeri, J. Kortus, and O. K. Andersen, Phys. Rev. Lett. **93**, 237002 (2004).
[26] X. Blase, C. Adessi, and D. Connétable, Phys. Rev. Lett. **93**, 237004 (2004).
[27] K.-W. Lee and W. E. Pickett, Phys. Rev. Lett. **93**, 237003 (2004).
[28] Y. Ma, J. S. Tse, T. Cui, D. D. Klug, L. Zhang, Y. Xie, Y. Niu, and G. Zou, Phys. Rev. B **72**, 014306 (2005).
[29] F. Giustino, Jonathan R. Yates, I. Souza, M. L. Cohen, and G. Louie, Phys. Rev. Lett. **98**, 047005 (2007).
[30] B. Sacépé, C. Chapelier, C. Marcenat, J. Kačmarčik, T. Klein, F. Omnès, and E. Bustarret, Phys. Status Solidi A **203**, 3315 (2006).
[31] P. Achatz, F. Omnès, L. Ortéga, C. Marcenat, J. Vacík, V. Hnatowicz, U. Köster, F. Jomard, and E. Bustarret, Diam. Relat. Mater. **19**, 814 (2010).
[32] See Supplemental Material at http://link.aps.org/supplemental/10.1103/PhysRevLett.119.017001 for the individual IXS scans, the full nonadiabatic phonon dispersion relations, and a comparison of theoretical and experimental linewidths.
[33] J. Kulda, H. Kainzmaier, D. Strauch, B. Dorner, M. Lorenzen, and M. Krisch, Phys. Rev. B **66**, 241202 (2002).
[34] Calculations were performed using density-functional theory [35,36] within the Perdew-Burke-Ernzerhof generalized-gradient approximation [37] for the exchange-correlation functional, as implemented in Quantum Espresso [38]. We used a plane-wave basis set with a kinetic energy cutoff of 60 Ry, norm-conserving Goedecker-Hartwigsen-Hutter-Teter pseudopotentials [39], and a $8 \times 8 \times 8$ Monkhorst-Pack grid for sampling the Brillouin zone. Adiabatic phonon frequencies and eigenvectors were computed through density-functional perturbation theory [40] on a $6 \times 6 \times 6$ grid. Electron bands, phonon dispersions, and electron-phonon matrix elements were interpolated using maximally localized Wannier functions [41,42], and Eq. (1) was computed using EPW V4 [43,44]. The Brillouin-zone summation in Eq. (1) was evaluated using one million random $\mathbf{k}$ points and a broadening parameter $\hbar\eta = 10$ meV. In all calculations, doping with boron was modeled in the rigid-band approximation through a shift of the Fermi level below the valence band top. A temperature of 300 K was included via the Fermi-Dirac occupation factors in Eq. (1). To approximately account for finite energy and momentum resolution, the results of Eqs. (2) and (3) were broadened by $\Delta E = 1$ meV and $\Delta k = 0.08$ Å^{-1} via a Gaussian convolution.
[35] P. Hohenberg and W. Kohn, Phys. Rev. **136**, B864 (1964).
[36] W. Kohn and L. J. Sham, Phys. Rev. **140**, A1133 (1965).
[37] J. P. Perdew, K. Burke, and M. Ernzerhof, Phys. Rev. Lett. **77**, 3865 (1996).

[38] P. Giannozzi *et al.*, J. Phys. Condens. Matter **21**, 395502 (2009).
[39] C. Hartwigsen, S. Goedecker, and J. Hutter, Phys. Rev. B **58**, 3641 (1998).
[40] S. Baroni, S. de Gironcoli, A. Dal Corso, and P. Giannozzi, Rev. Mod. Phys. **73**, 515 (2001).
[41] N. Marzari, A. A. Mostofi, J. R. Yates, I. Souza, and D. Vanderbilt, Rev. Mod. Phys. **84**, 1419 (2012).
[42] A. A. Mostofi, J. R. Yates, Y.-S. Lee, I. Souza, D. Vanderbilt, and N. Marzari, Comput. Phys. Commun. **178**, 685 (2008).
[43] F. Giustino, M. L. Cohen, and S. G. Louie, Phys. Rev. B **76**, 165108 (2007).
[44] S. Poncé, E. Margine, C. Verdi, and F. Giustino, Comput. Phys. Commun. **209**, 116 (2016).
[45] C. D. Clark, P. J. Dean, and P. V. Harris, Proc. R. Soc. A **277**, 312 (1964).
[46] S. Zollner, M. Cardona, and S. Gopalan, Phys. Rev. B **45**, 3376 (1992).
[47] E. Bustarret, F. Pruvost, M. Bernard, C. Cytermann, and C. Uzan-Saguy, Phys. Status Solidi A **186**, 303 (2001).
[48] M. Ortolani, S. Lupi, L. Baldassarre, U. Schade, P. Calvani, Y. Takano, M. Nagao, T. Takenouchi, and H. Kawarada, Phys. Rev. Lett. **97**, 097002 (2006).
[49] W. L. McMillan, Phys. Rev. **167**, 331 (1968).
[50] P. B. Allen and R. C. Dynes, Phys. Rev. B **12**, 905 (1975).
[51] D. J. Scalapino, Y. Wada, and J. C. Swihart, Phys. Rev. Lett. **14**, 102 (1965).